Geophysical Research Letters

RESEARCH LETTER
10.1029/2024GL109709

Multiday Soil Moisture Persistence and Atmospheric Predictability Resulting From Sahelian Mesoscale Convective Systems

C. M. Taylor[1,2], C. Klein[1], and B. L. Harris[1,2]

[1]UK Centre for Ecology and Hydrology, Wallingford, UK, [2]National Centre for Earth Observation, Wallingford, UK

Key Points:

- Satellite observations over the Sahel reveal how the land surface evolves in the 20 days after a Mesoscale Convective System (MCS)
- After an MCS, rainfall is suppressed over wet soils for 2 days in humid regions and up to 8 days in drier areas
- Initially soil moisture enhances rainfall predictability, but the strong land feedback degrades skill at longer lead times

Supporting Information:

Supporting Information may be found in the online version of this article.

Correspondence to:

C. M. Taylor,
cmt@ceh.ac.uk

Citation:

Taylor, C. M., Klein, C., & Harris, B. L. (2024). Multiday soil moisture persistence and atmospheric predictability resulting from sahelian mesoscale convective systems. *Geophysical Research Letters*, *51*, e2024GL109709. https://doi.org/10.1029/2024GL109709

Received 11 APR 2024
Accepted 9 OCT 2024

Abstract Skill in predicting where damaging convective storms will occur is limited, particularly in the tropics. In principle, near-surface soil moisture (SM) patterns from previous storms provide an important source of skill at the mesoscale, yet these structures are often short-lived (hours to days), due to both soil drying processes and the impact of new storms. Here, we use satellite observations over the Sahel to examine how the strong, locally negative, SM-precipitation feedback there impacts rainfall patterns over subsequent days. The memory of an initial storm pattern decays rapidly over the first 3–4 days, but a weak signature is still detected in surface observations 10–20 days later. The wet soil suppresses rainfall over the storm track for the first 2–8 days, depending on aridity regime. Whilst the negative SM feedback initially enhances mesoscale rainfall predictability, the transient nature of SM likely limits forecast skill on sub-seasonal time scales.

Plain Language Summary Early warning of severe weather is particularly important in Africa, where resilience to storm hazards such as flash flooding is weak. Given large-scale atmospheric conditions favorable for convective activity, understanding where storms will occur is challenging for conventional weather prediction models. In semi-arid regions such as the Sahel, the spatial distribution of SM provides additional predictability of convective rain, via its impact on heating and moistening of the atmosphere. Given that convection is favored over drier soils and that storms create new SM patterns every few days during the wet season, the extent to which knowledge of today's SM aids rainfall prediction in future days is unclear. Here we use 17 years of satellite observations to document how surface properties evolve over 20 days after a storm, and how the surface influences subsequent rainfall patterns. We find that even in regions of West Africa where storms are frequent, the suppression of rain over recently-wetted soils is evident out to 2 days. In climatologically drier regions, this predictability extends out to 8 days. Overall, the feedback between SM and rainfall enhances rainfall predictability in the short-term (days), but effectively degrades the skill of longer-term (weeks) forecasts.

1. Introduction

Across much of the world, soil moisture (SM) has an important influence on weather and climate through its control on energy and water fluxes into the atmosphere (Koster et al., 2004; Seneviratne et al., 2010). The lower atmosphere warms and dries in response to SM deficits, triggering impacts on convective cloud and rainfall, either directly via changes in thermodynamic stability (Bhowmick & Parker, 2018; Findell & Eltahir, 2003), or via circulation responses (Taylor et al., 2007). With a persistence time scale of days to months, SM anomalies provide predictability of future rain events (Dirmeyer et al., 2018; Koster et al., 2011). Realising land-based skill in practice is challenging for today's Numerical Weather Prediction (NWP) systems, due to difficulties in accurately specifying the initial state of the land surface, realistically simulating SM dynamics and their control on surface fluxes, and the impact of precipitation forecast biases on SM evolution.

A key element of land-based predictability is its spatial structure—individual rain events create highly heterogeneous SM fields, which in turn induce horizontal variability on scales of a few kilometres upwards within the lower atmosphere. Heterogeneous SM patterns have been shown to influence where new convective storms initiate in water-limited regimes across the world (Chug et al., 2023; Taylor et al., 2011). They provide a unique source of skillful prediction at these spatial scales, of particular value given the difficulties in predicting where hazardous convective storms will occur (Taylor et al., 2022).

10.1029/2024GL109709

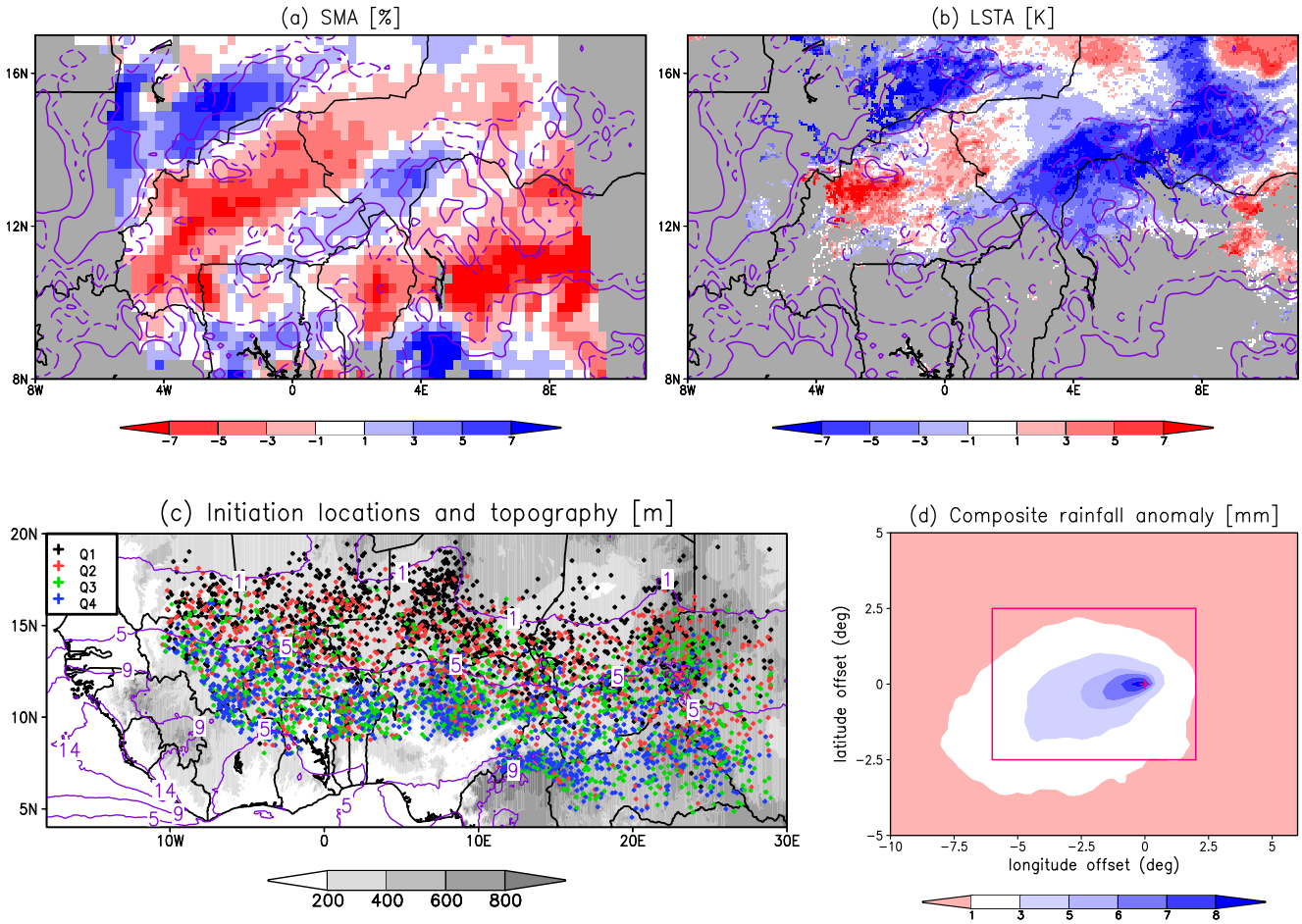

Figure 1. Example of antecedent Mesoscale Convective System (MCS) impacts on (a) soil moisture anomalies (%) based on AMSR-E data, and (b) LSTA (K) from the case study of Taylor et al. (2007). Dashed and solid purple contours indicate 48-hr antecedent rainfall of 10 and 25 mm. Gray shading: missing data due to satellite overpass (a) and cloud cover (b). (c) Study domain showing locations of MCS initiations, colored by rainfall in the previous 10 days (quartiles 1 to 4). Shading denotes topographic height (m) and purple contours show seasonal mean rainfall (mm day^{-1}). (d) 24-hr rainfall anomalies (mm) from compositing data relative to the initiation location I_0 (crimson cross) on day 0 for all MCSs. The MCS sub-domain used throughout the paper is defined by the rectangle.

How long SM anomalies persist (their "memory") affects how rapidly the skill of a mesoscale forecast decays. The memory is influenced by the characteristic time it takes the surface to dry out—weeks or months where deep-rooted vegetation is abundant, and much shorter in sparsely-vegetated semi-arid regions (Gallego-Elvira et al., 2016). It also depends on the frequency of rain events. The value of SM-derived skill for predicting the location of hazardous storms is likely greatest when such storms are frequent. However, rainy season skill tends to be shorter-lived, due to the frequency of new storms disrupting the initial SM pattern.

Here, we use satellite observations to examine how SM memory influences predictability of convection in the Sahel, a global hotspot of SM feedbacks on precipitation (hereafter SM-P; Koster et al., 2004; Taylor et al., 2012)). During the rainy season (June–September, JJAS), the surface rapidly moistens and vegetation develops. Over this period, surface fluxes move from being dominated by sensible (H) to latent heat (LE), but embedded in the seasonal evolution are high frequency fluctuations in evaporative fraction driven by evaporation direct from the soil over 1–2 days after rain (Lohou et al., 2014). Most rain comes from Mesoscale Convective Systems (MCSs; Mathon et al., 2002), typically initiating in the afternoon and growing to scales of several hundred kilometres, propagating westward. Typical systems have lifetimes less than 24 hr, but some continue for a second day (Futyan & Genio, 2007). They leave characteristic swaths of wet soil elongated in the direction of travel, many hundreds of kilometres in length. An illustration of MCS patterns and their impact on surface SM and Land Surface Temperature (LST) is provided in Figures 1a and 1b. Statistically, MCSs are favored ahead of the trough of African Easterly Waves (AEWs; Fink & Reiner, 2003; Reed et al., 1977), the dominant mode of

synoptic variability, and tend to produce rain at a given location every 3–4 days. This is evidenced by a negative lag-1 autocorrelation of daily rain (Roehrig et al., 2013), a globally unusual characteristic.

One can imagine that the evolution of the coupled land-atmosphere system over multiple days may lie somewhere between two extremes, with important implications for predictability of storms. At one end of the spectrum, the negative SM-P feedback dominates, initiating and sustaining MCSs over drier soil every afternoon/evening, reversing or at least equalizing the initial SM gradient. This kind of behavior is discussed by Hsu et al. (2017) and has been found in idealized models where external large-scale atmospheric variability is suppressed (Emori, 1998; Hohenegger & Stevens, 2018 at larger spatial scales). At this extreme, the timing and location of storms at the mesoscale is highly predictable for as long as the SM pattern exists. At the other end of the spectrum, atmospheric processes dominate, with synoptic scale variability (notably AEWs) determining when it rains, and the highly stochastic MCS dynamics controlling where it rains (Vogel et al., 2021). Here, MCS timing is dominated by synoptic forcing but the location is inherently unpredictable.

We use multi-year observations to understand how SM-P feedbacks influence where the Sahel sits on this predictability spectrum. This is achieved by mapping variability in surface properties and rainfall in the days after an MCS. The spatial fingerprint of the initial MCS allows us to pinpoint the extent to which local (land) forcing influences convection within larger-scale atmospheric variability.

2. Data and Methods

We analyze data from the Meteosat Second Generation (MSG) series of geostationary satellites over West Africa for JJAS from 2004 to 2020. These data have a spatial resolution ∼3 km and are available every 15 min. We use the cloud-top temperature field from MSG channel 9 (10.8 microns) to identify MCS initiations during the afternoon and evening (1400–2100 UTC). Following Taylor et al. (2011), initiations are defined by the appearance of new cold cloud structures (−40°C threshold) exceeding 5,000 km^2 in area. Each new MCS is tracked forward in time, based on overlapping cold cloud in consecutive images (Klein & Taylor, 2020), until the area drops below 5,000 km^2. We only retain MCSs with a lifetime of at least 6 hr, and containing at least one convective core (as identified by wavelet analysis; Klein et al., 2018) at each time step. Subsequent analysis is performed on a rectangular sub-domain around each initiation, extending 8° in longitude and 5° in latitude, dimensions motivated by characteristic MCS swath sizes. Cases where this sub-domain crosses a coastline are excluded. This approach yields 5545 MCSs (Figure 1c) which we split into quartiles based on sub-domain mean rainfall in the 10 days preceding the MCS event. The 10-day accumulation period effectively filters out the impact of short dry spells on root zone SM, and our results are insensitive to alternative periods of 5 and 15 days. Sub-setting provides a simple proxy method to split cases according to regional soil wetness, implicitly accounting for variability in location and time of year.

Rainfall is taken from version 6 of the Integrated Multi-satellitE Retrievals for GPM product (IMERG), based on a combination of thermal infra-red and microwave imagery, corrected with gauge observations. We create fields of 24-hr rainfall accumulation from 1200 UTC using the half-hourly images. Note that within our domain, local solar time lies within 2 hr of UTC.

To identify how the land surface evolves in response to MCSs, we exploit three independent observational data sets characterizing different aspects of land surface state. We use the surface SM index created by the Hydrology Science Applications Facility (H-SAF, 2020). This is derived using microwave backscatter from the Advanced Scatterometer (ASCAT) instrument on the Metop satellite series. It provides typically once-daily data around 0930 or 2130 LT from 2007 onwards at a resolution of 0.25°. Information on vegetation water content due to changes in both vegetation structure (e.g., changes in leaf area) and leaf level water content comes from passive microwave Vegetation Optical Depth (VOD) data. We use the 0.25° X-band product from the VOD Climate Archive (Moesinger et al., 2020), with nocturnal observations available on 70%–80% of days up to 2018. Finally, satellite-derived LSTs constitute a direct measurement of the surface energy balance. Daytime LST data in semi-arid regions provide a valuable observational proxy for the partition between sensible and latent heat fluxes. We use the Land SAF LST product from MSG sampled every 15 min wherever cloud-free conditions are detected (Sobrino & Romaguera, 2004). Following Taylor et al. (2007), daily LST anomalies (hereafter LSTA) are computed for each 3 km pixel based on the mean of all cloud-free observations (relative to a long-term climatology) between 0700 and 1,700. Additional cloud screening is applied (Talib et al., 2022) to minimize the impact of misdiagnosed cloud-free conditions within the pixel. The LST climatology covers the period 2004–15. Note

that the data sets contain missing values due to a combination of cloud (LST), incomplete satellite overpass coverage (SM, VOD), and data set length (SM, VOD). However, consistent behavior emerges across variables when averaging over thousands of MCSs, even when individual events are not sampled in all data sets.

All data are put on a common $0.25 \times 0.25°$ grid, and sub-grid heterogeneity is quantified by the standard deviation of LSTA within each grid-cell. In Section 3.2, we spatially composite the various data sets relative to the initiation location (I_0) of each MCS. Figure 1d illustrates the resulting composite mean 24-hr rainfall accumulation (starting at 1200 UTC; hereafter MCS_0), having first subtracted the climatological daily rainfall for each grid point. This depicts a clear "initial" rainfall anomaly pattern extending westwards over 500 km from I_0. To ensure we only composite events with similar initial rainfall patterns, we use K-means clustering on the MCS_0 field to create 5 distinct clusters, distinguishing intense, long-lived (C1,2) and merged or short-lived (C3-5) systems (Figure S1 in Supporting Information S1).

3. Results

3.1. Time-Lagged Spatial Correlation Analysis

To provide a consistent quantification of the memory of spatial patterns across different variables and time lags, we perform a spatial correlation between the MCS_0 daily rainfall anomaly and our variable of interest across the event sub-domain for each MCS in the data set. We analyze the lagged correlation from day 0 (i.e., event day) out to 20 days afterward. For a given variable and lag, each case yields a Pearson correlation coefficient r. We sub-divide the 5,545 events into antecedent rainfall quartiles (Figure 1c), and compare the mean coefficient within each quartile (r_e) against a non-event sample of coefficients r_{ne}. The latter are computed from correlating the original event rainfall anomalies with the variable at the same lag (sampled on the same day of year) but in a randomly selected different year. Comparing r_e with r_{ne} implicitly accounts for the effects of spatial autocorrelation and seasonality of variables, which are present in both samples. We repeat this process 1,000 times, and from the resulting distribution of r_{ne} we compute the likelihood of obtaining a value as extreme as r_e based on a two-tailed test.

We first consider SM sampled at 0930LT ahead of MCS_0 initiation (day 0; Figure 2a), where there is a significant negative correlation for all quartiles between the event rainfall pattern and its antecedent SM, consistent with a negative spatial feedback between SM and rainfall (Guillod et al., 2015; Taylor et al., 2012). Large positive correlations are recorded on day 1, ordered by quartile, and are consistent with a strong SM response to MCS_0. Correlations decrease rapidly over the next 3 days, but remain significantly positive out to day 20, with the exception of several long-lags in the wettest two quartiles. This evolution of r_e is mirrored in the lagged LSTA correlation, with significant negative pattern correlations dominating out to day 20 (Figure 2b). This indicates that even 20 days after MCS_0, there is a small but detectable suppression of LST (consistent with enhanced evapotranspiration) over the wettest pixels compared to their drier neighbors. The lagged impact on VOD (Figure 2c) indicates a more complex transition from negative correlations in the days after MCS_0 toward positive correlations. We interpret the somewhat surprising initial apparent negative response of vegetation water content to rainfall as an artifact caused by the effects of surface water on the brightness temperature used for the VOD retrieval. Even small fractions of surface inundation are known to result in artificial reductions in inferred VOD (Bousquet et al., 2021; Harris et al., 2022). Increased surface inundation is expected in wetter conditions, explaining the longer-lived negative VOD correlations in Q3 and Q4. In the less-contaminated, drier quartiles there is a significant and sustained increase in VOD out to 20 days in the areas most affected by MCS_0. Rain from MCS_0 induces a spatial pattern of increased leaf water and/or leaf area which persists, and likely helps to maintain enhanced evapotranspiration over that period. Finally, we consider the lagged autocorrelation of daily rainfall patterns (Figure 2d). In all quartiles there is a significant negative spatial correlation of rainfall on days 1 and 2. That is, for the 2 days after MCS_0, rainfall is favored in locations which received less rain originally. As with the other variables, the signal is strongest for the driest quartile. Indeed, excluding day 4, rainfall patterns in Q1 remain significantly negatively correlated out to day 8, indicating a surprisingly long-lived negative feedback. The correlation sensitivity to initial wetness is expected for two reasons. Firstly, evapotranspiration in wetter regimes (Q3,4) tends to be less sensitive to the additional water supplied by MCS_0. Secondly, those regimes tend to have more frequent storms climatologically, implying that SM anomalies will degrade more rapidly due to new rain events.

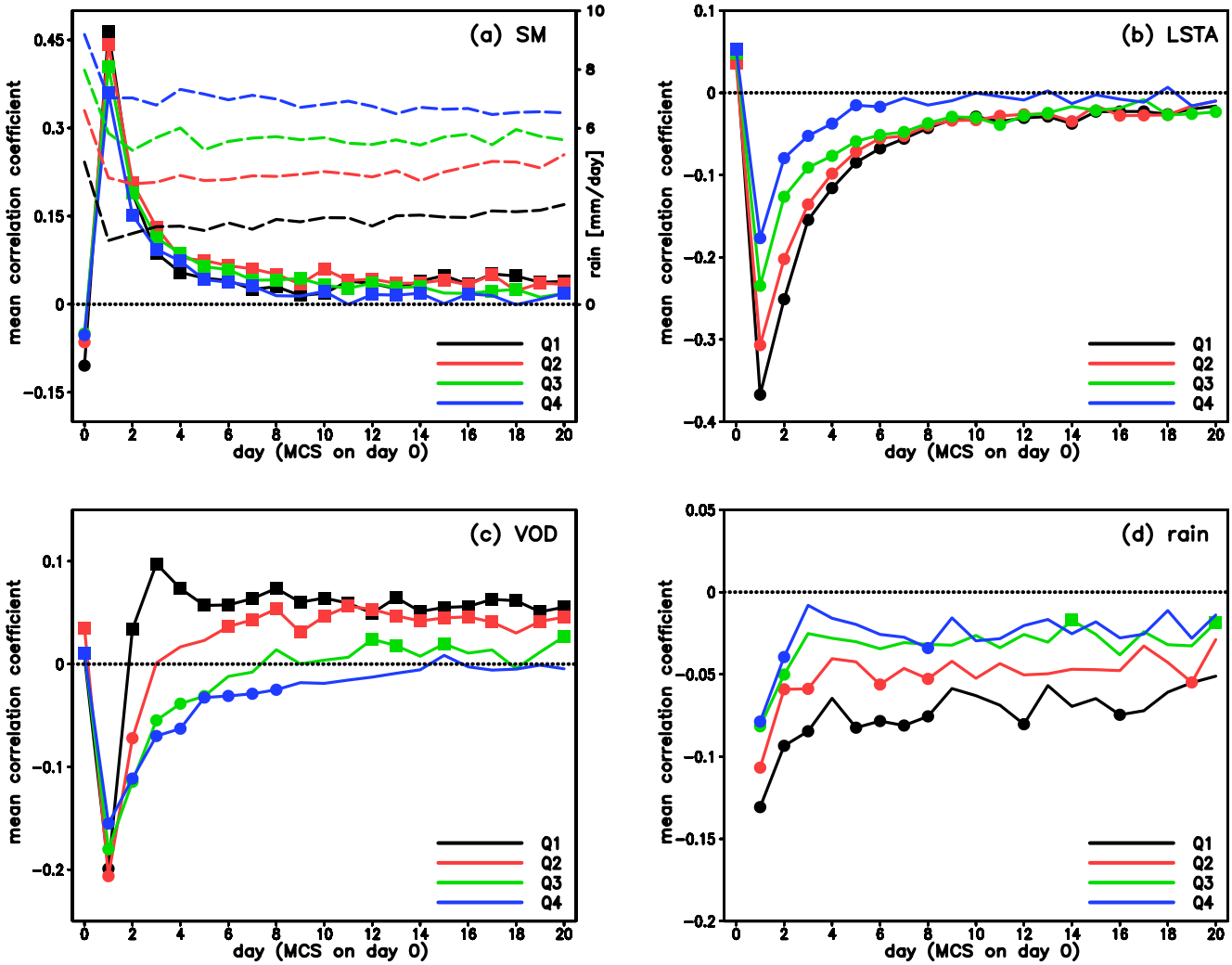

Figure 2. Mean spatial correlation coefficients r_e between MCS_0 rainfall and lagged (a) soil moisture, (b) LSTA, (c) Vegetation Optical Depth and (d) subsequent rainfall. The results are split into quartiles Q1 (driest) to Q4 (wettest) in terms of 10-day antecedent rain. Significant deviations of r_e from the non-event distribution r_{ne}, at the 5% level are indicated by squares (positive) and circles (negative correlations). Mean daily rainfall (mm) is indicated by dashed lines in panel (a).

3.2. Composite Analysis

We now examine the post-MCS space-time evolution of the coupled land-atmosphere system using a composite approach. To focus on conditions where memory effects are strong, we restrict the analysis to the driest two quartiles, and present primary results from the cluster with the largest amplitude composite-mean MCS_0 signal (C1; Figure 3d). The cluster contains 633 events (11% of the total) and closely resembles the all-event mean in Figure 1d. It is representative of a typical long-lived MCS, with a rainfall pattern stretching ~1,000 km toward the south-west. Composite results from the remaining clusters are presented in Supporting Information S1.

In terms of the surface pattern preceding MCS_0, the composite mean LSTA field (Figure 3a) indicates a strong preference for MCS initiation and propagation over warm (and dry) soils, consistent with Taylor et al. (2011) and Klein and Taylor (2020). In the 2 days after MCS_0 (Figure 3b), there is a large amplitude reversal in LSTA, maximized over the area of heaviest rainfall. This weakens over the next 2 days (Figure 3c) but a clear pattern of significant negative LSTAs remains to the south-west of I_0. These MCS-scale LSTA patterns are anti-correlated with SM anomalies (Figure S2 in Supporting Information S1), as expected. The overall suppression of rainfall on days 1–2 over surfaces wetted by MCS_0, as implied by Figure 2d, is clearly seen in the composite rainfall (Figure 3e). Across the south-west of the domain, rainfall deficits exceeding 1 mm/day (compared to a climatology of typically 3–5 mm/day) emerge. Averaged across the MCS sub-domain, this leads to a marked day 1

10.1029/2024GL109709

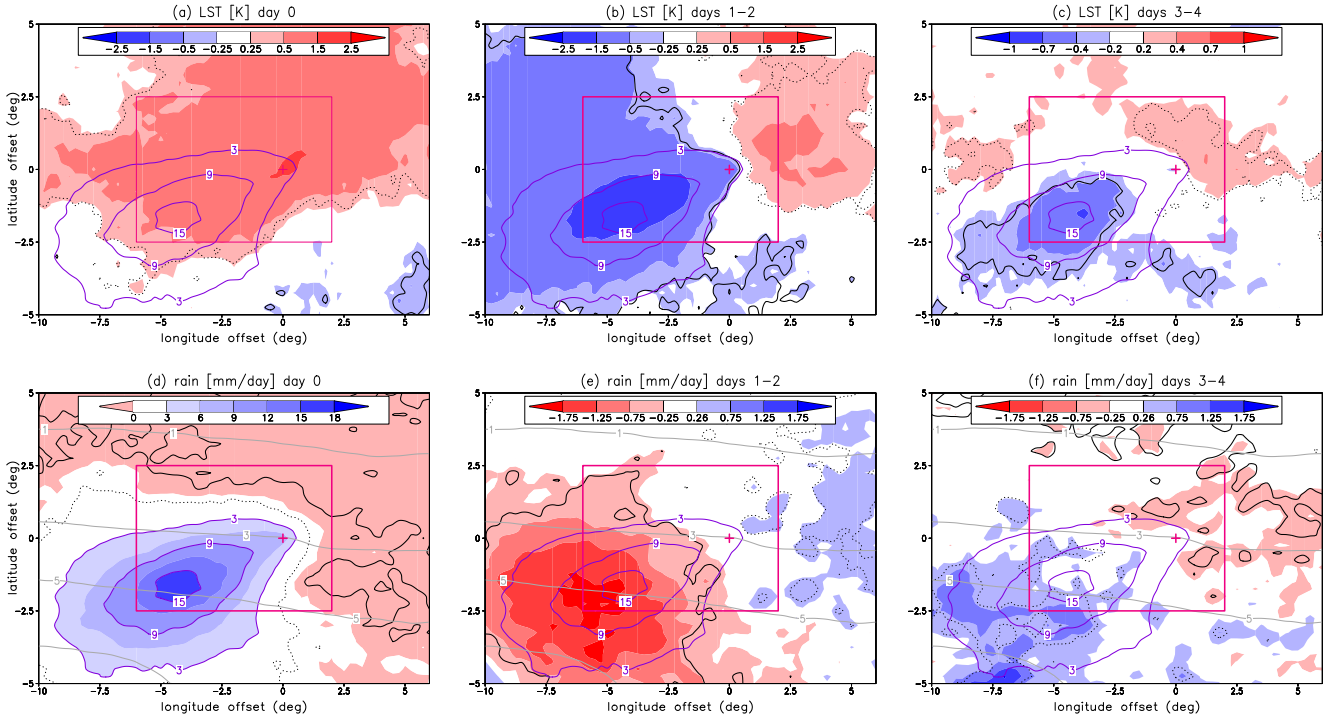

Figure 3. Spatial composites from the driest two quartiles of cluster C1 of LSTA (a, b, and c) and rainfall (d, e, and f) on day 0 (a, d), and averaged over days 1–2 (b, e) and 3–4 (c, f). Values significantly less (more) than a control sample at the 95% level are enclosed by solid (dotted) contours. Purple (gray in d–f) contours denote event (climatological daily) rainfall (mm).

rainfall reduction (Figure 2a), and to a lesser extent day 2. In the frame of reference of a westward-propagating MCS, the suppression of rainfall increases (in absolute terms) with distance traveled over the recently-wetted surface, consistent with previous findings (Klein & Taylor, 2020; Taylor et al., 2018) that MCSs progressively weaken over extensive wet surfaces. Similar reductions in rainfall over wet soil during days 1–2 are also evident in clusters C2–C4 (Figures S3–S5e in Supporting Information S1), and the wettest cases in cluster C1 (Figure S7e in Supporting Information S1). This local rainfall suppression points unambiguously to land-atmosphere feedback. Modulation of convection by synoptic processes would not produce such a localized response. Similarly, local atmospheric memory of the MCS, for example, linked to vertical mixing, extensive cloud shields and cold pools, is expected to degrade in the hours after an MCS, particularly in the presence of strong nocturnal advection (Schwendike et al., 2010).

The overall rainfall response on days 3 and 4 is distinct from days 1 and 2 (Figure 3f). There are areas of weak, and sometimes significant, rainfall enhancement around the downstream (south–western) edges of MCS_0 which resemble a halo. Across the upstream side of the MCS_0 wet swath, rainfall is close to climatology. An important factor to consider here is the role of the large-scale in sequencing convective activity. With a typical AEW frequency of 3–4 days, our composite, defined by MCSs at day 0, will likely contain more MCS-favorable synoptic conditions on days 3–4, resulting in widespread positive rainfall anomalies. However, significant areas of enhanced convection on these days are only found away from the rainiest MCS_0 pixels, consistent with negative pattern correlations in Figure 2d. Taken together, whilst this implies an important role for synoptic variability in the timing of convection, residual local rainfall suppression via negative SM-P feedback still provides some spatial predictability 3–4 days after MCS_0 within this cluster. Consistent with this, there is weak day 3–4 rainfall suppression over, and/or enhancement around, wet soils in clusters C2 and C3 (Figures S3–S4f in Supporting Information S1). The amplitude of the MCS_0 rainfall in clusters C4 and C5 (Figures S5–S6 in Supporting Information S1) is not large enough to maintain an extensive negative LSTA signal by days 3–4, leading to a more rapid decay of coherent land memory impacts on rainfall in these cases.

Finally, we examine the spatial patterns in land variables and rainfall indicative of extended memory between 5 and 20 days after the initial event, based on cluster C1. Averaged over this period, there is a weak (~-0.2 K) but

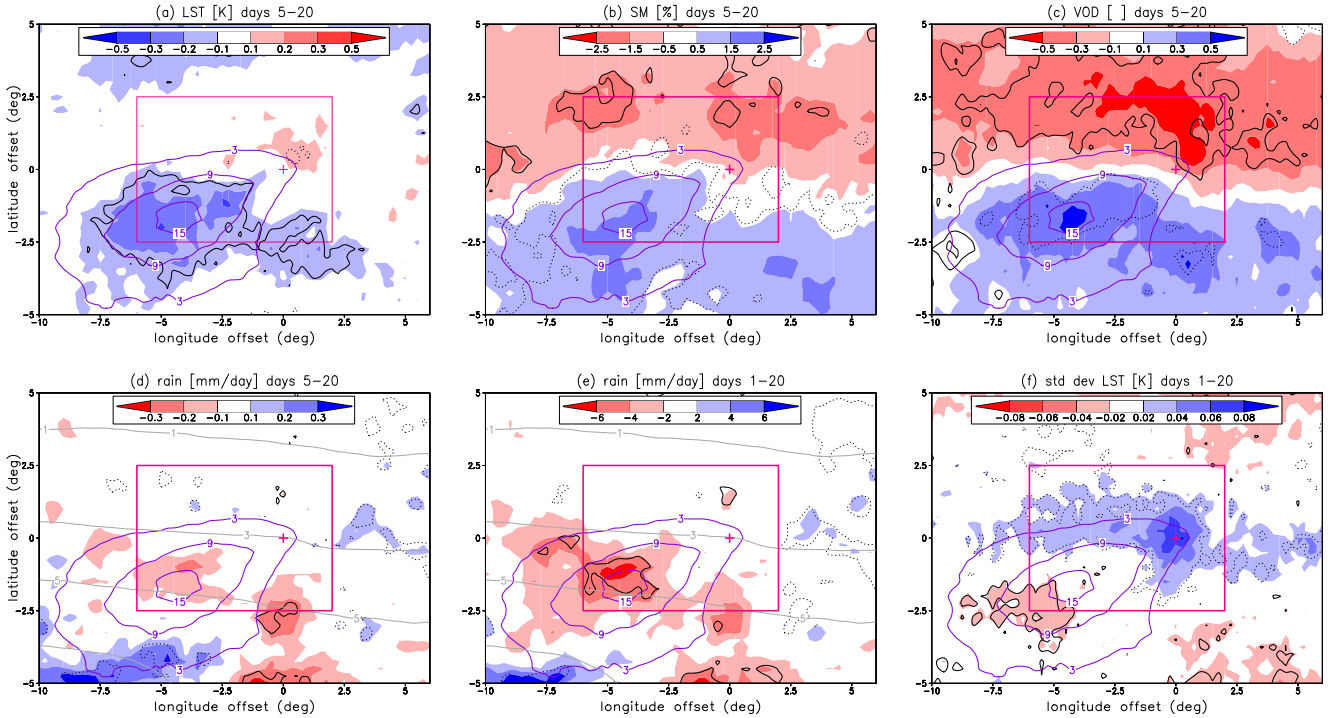

Figure 4. As for Figure 3 but showing anomalies in LSTA (a), soil moisture (b), Vegetation Optical Depth (c) and rainfall (d) averaged from day 5–20 after the Mesoscale Convective System (MCS) event. Cumulative rainfall (e) and spatial standard deviation in LSTA (f) averaged over 20 days after the MCS.

significant LSTA signal over and to the south-west of MCS_0 (Figure 4a). A similar MCS-scale structure is evident in positive SM and VOD anomalies, superimposed on a weaker, large-scale meridional signal. There is a suggestion of a continued weak halo effect in the south-west considering rainfall averaged over these 16 days (Figure 4d). Figure 4e shows the cumulative rainfall over all 20 days after MCS_0. This highlights a significant suppression of rain over the central (wettest) region of MCS_0 of up to 6 mm. Comparing with MCS_0 totals in that region ~10–18 mm, it is clear that the net rainfall pattern remains dominated by MCS_0, rather than any subsequent rainfall response. It is notable in Figure 4e that there is no widespread positive rainfall anomaly in the 20 days after MCS_0.This lack of evidence for a sustained positive SM-P feedback across the MCS swath raises questions about positive feedbacks reported at monthly and seasonal time scales in the Sahel (e.g., Los et al., 2006; Yu et al., 2017), though it is possible that other processes become important at the monsoon scale (several 1,000 km). Interestingly, MCS_0 also creates a significant enhancement of sub-grid surface heterogeneity across its northern edge, maximized around I_0 (Figure 4f), which persists over 20 days, and may influence convective initiation (Hsu et al., 2017; Taylor et al., 2011).

4. Summary and Discussion

From independent satellite observations, we have shown that a memory of MCS patterns in land surface properties is still evident 20 days later. However, the amplitude weakens rapidly in the first 3–4 days, especially in wetter conditions. Consistent with this, and previous studies showing strong organization of rainfall over drier soils, we find subsequent rainfall favored over drier surfaces compared to the main MCS-affected area. The lagged effect on rainfall is clear in all wetness regimes for 2 days, and extends to 8 days in drier regimes. There is also evidence of modest spatial redistribution of rainfall patterns in the 20 days following a typical MCS, with rainfall decreases over the wettest soils.

The persistence of land memory for 2 weeks or more, albeit weak beyond the first few days, sheds light on where the Sahel sits between the two extreme scenarios previously outlined. In spite of a clear negative SM-P feedback, MCS-induced SM anomalies are not rapidly reversed or even equalized, as would be the case with a dominant land feedback. The real world does not behave like highly idealized simulations where large-scale atmospheric variability is suppressed (e.g., Emori, 1998; Hohenegger & Stevens, 2018), at least on scales of hundreds of

kilometres. The other extreme scenario considered, whereby mesoscale rainfall patterns are inherently unpredictable, is also refuted. Marked local rainfall suppression over wet soils for 2 days after an MCS can only be explained by the persistent spatial forcing that SM provides. Indeed, it seems likely that SM-P feedbacks contribute to the observed negative lag-1 autocorrelation of daily rain (Roehrig et al., 2013).

What does this mean for predictability of rainfall beyond the nowcasting time scale? It is well-known that synoptic-scale atmospheric variability provides predictive skill for West African rainfall at large scales (Peyrillé et al., 2023; Schlueter et al., 2019). The multi-day persistence of land surface heterogeneity in the aftermath of an MCS provides an important complementary source of rainfall predictability at finer, user-relevant scales. We show that the latter is evident out to 48 hr under all wetness regimes sampled here (Figure 2d). During drier periods for example, outside of the peak monsoon season or in the Northern Sahel, land memory provides predictability out to 8 days ahead. Lack of a Sahelian positive SM-P feedback at MCS scale over 20 days raises questions about strong positive feedbacks implied in previous statistical studies at monthly and monsoon scale. By examining processes at high space and time resolution, the evidence here indicates that the dominant feedback is negative whenever strong SM gradients and favorable synoptic conditions coincide, and there is no upscale positive feedback.

Data Availability Statement

This study uses freely-available data derived from satellites; cloud-top temperature imagery from Eumetsat (https://user.eumetsat.int/catalogue/EO:EUM:DAT:0156; soil moisture from the Hydrology SAF (https://hsaf.meteoam.it/Products/Detail?prod=H119); Land Surface Temperature from the Land SAF (https://datalsasaf.lsasvcs.ipma.pt/PRODUCTS/MSG/MLST/; Vegetation Optical Depth from the Global Long-term Microwave VOD Climate Archive (Moesinger et al., 2019); IMERG rainfall rates (NASA, 2020). The algorithm for identification of convective cores is freely- available (Klein, 2024). Spatial relationships between land surface temperature, soil moisture, convective cores and precipitation can be visualized for the most recent years at https://eip.ceh.ac.uk/hydrology/sub-saharan-africa/nowcasting/.

Acknowledgments
This research was funded by UK Research and Innovation GCRF under the African SWIFT project (NE/P021077/1) and the Natural Environment Research Council (NE/W001888/1, NE/X006247/1).

References

Bhowmick, M., & Parker, D. J. (2018). Analytical solution to a thermodynamic model for the sensitivity of afternoon deep convective initiation to the surface Bowen ratio. *Quarterly Journal Of The Royal Meteorological Society*, *144*(716), 2216–2229. https://doi.org/10.1002/qj.3340

Bousquet, E., Mialon, A., Rodriguez-Fernandez, N., Prigent, C., Wagner, F. H., & Kerr, Y. H. (2021). Influence of surface water variations on VOD and biomass estimates from passive microwave sensors. *Remote Sensing of Environment*, *257*, 112345. https://doi.org/10.1016/j.rse.2021.112345

Chug, D., Dominguez, F., Taylor, C. M., Klein, C., & Nesbitt, S. W. (2023). Dry-to-Wet soil gradients enhance convection and rainfall over subtropical South America. *Journal of Hydrometeorology*, *24*(9), 1563–1581. https://doi.org/10.1175/JHM-D-23-0031.1

Dirmeyer, P. A., Halder, S., & Bombardi, R. (2018). On the harvest of predictability from land states in a global forecast model. *Journal of Geophysical Research: Atmospheres*, *123*(23), 13–111. https://doi.org/10.1029/2018JD029103

Emori, S. (1998). The interaction of cumulus convection with soil moisture distribution: An idealized simulation. *Journal of Geophysical Research*, *103*(D8), 8873–8884. https://doi.org/10.1029/98jd00426

Findell, K. L., & Eltahir, E. A. B. (2003). Atmospheric controls on soil moisture-boundary layer interactions. Part I: Framework development. *Journal of Hydrometeorology*, *4*(3), 552–569. https://doi.org/10.1175/1525-7541(2003)004<0552:acosml>2.0.co;2

Fink, A. H., & Reiner, A. (2003). Spatio-temporal variability of the relation between African easterly waves and West African squall lines in 1998 and 1999. *Journal of Geophysical Research*, *108*(D11). https://doi.org/10.1029/2002jd002816

Futyan, J. M., & Genio, A. D. D. (2007). Deep convective system evolution over Africa and the tropical Atlantic. *Journal of Climate*, *20*(20), 5041–5060. https://doi.org/10.1175/jcli4297.1

Gallego-Elvira, B., Taylor, C. M., Harris, P. P., Ghent, D., Veal, K. L., & Folwell, S. S. (2016). Global observational diagnosis of soil moisture control on the land surface energy balance. *Geophysical Research Letters*, *43*(6), 2623–2631. https://doi.org/10.1002/2016gl068178

Guillod, B. P., Orlowsky, B., Miralles, D. G., Teuling, A. J., & Seneviratne, S. I. (2015). Reconciling spatial and temporal soil moisture effects on afternoon rainfall. *Nature Communications*, *6*(1), 6443. https://doi.org/10.1038/ncomms7443

Harris, B. L., Taylor, C. M., Weedon, G. P., Talib, J., Dorigo, W., & van der Schalie, R. (2022). Satellite-observed vegetation responses to intraseasonal precipitation variability. *Geophysical Research Letters*, *49*(15), e2022GL099635. https://doi.org/10.1029/2022GL099635

Hohenegger, C., & Stevens, B. (2018). The role of the permanent wilting point in controlling the spatial distribution of precipitation. In *Proceedings of the national academy of sciences*. https://doi.org/10.1073/pnas.1718842115

H-SAF. (2020). ASCAT surface soil moisture climate data record v5 12.5 km sampling - Metop, EUMETSAT SAF on support to operational Hydrology and water management. https://doi.org/10.15770/EUM_SAF_H_0006

Hsu, H., Lo, M.-H., Guillod, B. P., Miralles, D. G., & Kumar, S. (2017). Relation between precipitation location and antecedent/subsequent soil moisture spatial patterns. *Journal of Geophysical Research: Atmospheres*, *122*(12), 6319–6328. https://doi.org/10.1002/2016jd026042

Klein, C. (2024). Cornkle/ccores: Research version (Version 1.0) [Software]. *Zenodo*. https://doi.org/10.5281/zenodo.11163050

Klein, C., Belušić, D., & Taylor, C. M. (2018). Wavelet scale analysis of mesoscale convective systems for detecting deep convection from infrared imagery. *Journal of Geophysical Research: Atmospheres*, *123*(6), 3035–3050. https://doi.org/10.1002/2017JD027432

Klein, C., & Taylor, C. M. (2020). Dry soils can intensify mesoscale convective systems. *Proceedings of the National Academy of Sciences* (Vol. 117(35), 21132–21137). https://doi.org/10.1073/pnas.2007998117

Koster, R. D., Dirmeyer, P. A., Guo, Z. C., Bonan, G., Chan, E., Cox, P., et al. (2004). Regions of strong coupling between soil moisture and precipitation. *Science*, *305*(5687), 1138–1140. https://doi.org/10.1126/science.1100217

Koster, R. D., Mahanama, S. P. P., Yamada, T. J., Balsamo, G., Berg, A. A., Boisserie, M., et al. (2011). The second phase of the global land–atmosphere coupling experiment: Soil moisture contributions to subseasonal forecast skill. *Journal of Hydrometeorology*, *12*(5), 805–822. https://doi.org/10.1175/2011jhm1365.1

Lohou, F., Kergoat, L., Guichard, F., Boone, A., Cappelaere, B., Cohard, J. M., et al. (2014). Surface response to rain events throughout the West African monsoon. *Atmospheric Chemistry and Physics*, *14*(8), 3883–3898. https://doi.org/10.5194/acp-14-3883-2014

Los, S. O., Weedon, G. P., North, P. R. J., Kaduk, J. D., Taylor, C. M., & Cox, P. M. (2006). An observation-based estimate of the strength of rainfall-vegetation interactions in the Sahel. *Geophysical Research Letters*, *33*(16). https://doi.org/10.1029/2006gl027065

Mathon, V., Laurent, H., & Lebel, T. (2002). Mesoscale convective system rainfall in the Sahel. *Journal of Applied Meteorology*, *41*(11), 1081–1092. https://doi.org/10.1175/1520-0450(2002)041<1081:mcsrit>2.0.co;2

Moesinger, L., Dorigo, W., De Jeu, R., Van der Schalie, R., Scanlon, T., Teubner, I., & Forkel, M. (2019). The global long-term microwave vegetation optical depth climate archive VODCA (version 1.0) [Dataset]. https://doi.org/10.5281/zenodo.2575599

Moesinger, L., Dorigo, W., de Jeu, R., van der Schalie, R., Scanlon, T., Teubner, I., & Forkel, M. (2020). The global long-term microwave Vegetation Optical Depth Climate Archive (VODCA). *Earth System Science Data*, *12*(1), 177–196. https://doi.org/10.5194/essd-12-177-2020

NASA. (2020). Global Precipitation Measurements (GPM) Integrated Multi-Satellite Retrievals (IMERG) L3 half hourly 0.1 degree x 0.1 degree (version 06) [Dataset]. https://catalogue.ceda.ac.uk/uuid/47c32530265d4d6e8fdb6c08b2330371

Peyrillé, P., Roehrig, R., & Sanogo, S. (2023). Tropical waves are key drivers of extreme precipitation events in the central Sahel. *Geophysical Research Letters*, *50*(20), e2023GL103715. https://doi.org/10.1029/2023GL103715

Reed, R. J., Norquist, D. C., & Recker, E. E. (1977). The structure and properties of African wave disturbances as observed during phase III of GATE. *Monthly Weather Review*, *105*(3), 317–333. https://doi.org/10.1175/1520-0493(1977)105<0317:tsapoa>2.0.co;2

Roehrig, R., Bouniol, D., Guichard, F., Hourdin, F., & Redelsperger, J.-L. (2013). The present and future of the West African monsoon: A process-oriented assessment of CMIP5 simulations along the AMMA transect. *Journal of Climate*, *26*(17), 6471–6505. https://doi.org/10.1175/jcli-d-12-00505.1

Schlueter, A., Fink, A. H., Knippertz, P., & Vogel, P. (2019). A systematic comparison of tropical waves over Northern Africa. Part I: Influence on rainfall. *Journal of Climate*, *32*(5), 1501–1523. https://doi.org/10.1175/jcli-d-18-0173.1

Schwendike, J., Kalthoff, N., & Kohler, M. (2010). The impact of mesoscale convective systems on the surface and boundary-layer structure in West Africa: Case-studies from the AMMA campaign 2006. *Quarterly Journal Of The Royal Meteorological Society*, *136*(648), 566–582. https://doi.org/10.1002/qj.599

Seneviratne, S. I., Corti, T., Davin, E. L., Hirschi, M., Jaeger, E. B., Lehner, I., et al. (2010). Investigating soil moisture-climate interactions in a changing climate: A review. *Earth-Science Reviews*, *99*(3–4), 125–161. https://doi.org/10.1016/j.earscirev.2010.02.004

Sobrino, J. A., & Romaguera, M. (2004). Land surface temperature retrieval from MSG1-SEVIRI data. *Remote Sensing of Environment*, *92*(2), 247–254. https://doi.org/10.1016/j.rse.2004.06.009

Talib, J., Taylor, C. M., Klein, C., Harris, B. L., Anderson, S. R., & Semeena, V. S. (2022). The sensitivity of the West African monsoon circulation to intraseasonal soil moisture feedbacks. *Quarterly Journal Of The Royal Meteorological Society*, *148*(745), 1709–1730. https://doi.org/10.1002/qj.4274

Taylor, C. M., de Jeu, R. A. M., Guichard, F., Harris, P. P., & Dorigo, W. A. (2012). Afternoon rain more likely over drier soils. *Nature*, *489*(7416), 423–426. https://doi.org/10.1038/nature11377

Taylor, C. M., Gounou, A., Guichard, F., Harris, P. P., Ellis, R. J., Couvreux, F., & De Kauwe, M. (2011). Frequency of Sahelian storm initiation enhanced over mesoscale soil-moisture patterns. *Nature Geoscience*, *4*(7), 430–433. https://doi.org/10.1038/ngeo1173

Taylor, C. M., Klein, C., Dione, C., Parker, D. J., Marsham, J., Abdoulahat Diop, C., et al. (2022). Nowcasting tracks of severe convective storms in West Africa from observations of land surface state. *Environmental Research Letters*, *17*(3), 034016. https://doi.org/10.1088/1748-9326/ac536d

Taylor, C. M., Parker, D. J., & Harris, P. P. (2007). An observational case study of mesoscale atmospheric circulations induced by soil moisture. *Geophysical Research Letters*, *34*(15), L15801. https://doi.org/10.1029/2007GL030572

Taylor, C. M., Prigent, C., & Dadson, S. J. (2018). Mesoscale rainfall patterns observed around wetlands in sub-Saharan Africa. *Quarterly Journal Of The Royal Meteorological Society*, *144*(716), 2118–2132. https://doi.org/10.1002/qj.3311

Vogel, P., Knippertz, P., Gneiting, T., Fink, A. H., Klar, M., & Schlueter, A. (2021). Statistical forecasts for the occurrence of precipitation outperform global models over northern tropical Africa. *Geophysical Research Letters*, *48*(3), e2020GL091022. https://doi.org/10.1029/2020GL091022

Yu, Y., Notaro, M., Wang, F., Mao, J., Shi, X., & Wei, Y. (2017). Observed positive vegetation-rainfall feedbacks in the Sahel dominated by a moisture recycling mechanism. *Nature Communications*, *8*(1), 1873. https://doi.org/10.1038/s41467-017-02021-1